Supercurrent peaks in planar high-temperature superconducting Josephson junctions

M. S. Rzchowski*
Physics Department, University of Wisconsin–Madison, 1150 University Avenue, Madison, Wisconsin 53706

B. A. Davidson
Physics Department, University of Illinois–Urbana Champaign, 1110 West Green Street, Urbana, Illinois 61801
(Received 1 May 2000)

We investigate the current-voltage (IV) characteristics of planar high-temperature superconducting Josephson junctions in the physically relevant overdamped limit. We show that the nonuniform bias current distribution induced by the planar geometry leads to unexpected modifications of the IV characteristic, including a resonancelike supercurrent peak that moves with applied magnetic field. We show that these are not resonance effects, but are due to a dynamical instability in the supercurrent distribution. All of the several bias distributions investigated result in the field-dependent supercurrent peaks.

I. INTRODUCTION

Many high-temperature superconductor (HTSC) Josephson junctions are fabricated with a geometry very close to planar, where the electrodes and the Josephson barrier lie exactly or approximately in the same plane. Grain boundary[1] and focused electron beam[2] junctions are exactly planar, while artificial barrier step-edge[3] junctions are very close to this geometry. In many HTSC systems, planar geometry effects have been discovered to induce modified critical-state behavior[4] and geometrical flux-entry barriers.[5] In a planar Josephson junction, the geometry of the junction influences the current-voltage (IV) characteristics when the critical current becomes large enough that transport currents contribute significantly to the magnetic field at the junction (the long junction limit). This in turn affects such fundamental information as the critical current density and its dependence on crystallographic orientation.

In this paper we report an additional unexpected effect: that the known nonuniform current distribution in the electrodes of planar Josephson junctions introduces unusual magnetic-field-dependent features into the IV characteristic, such as excess supercurrent and resonancelike structure. This occurs even in the overdamped limit characteristic of HTSC junctions. This effect will alter the true resonance structure that appears away from the overdamped limit, and hence will affect the derivation of microscopic properties from supercurrent resonances. We show that this is caused by an interesting transition, in a narrow region of bias current, between two qualitatively different dissipative states. We find the structure of the transition to be very similar to the transition between superconducting and dissipative states that occurs at the (lower) critical current.

In Sec. II, we introduce the problem and describe the focus of the paper. Section III describes the particular limiting case of edge-biased junctions, where the bias current is concentrated entirely at the two junction ends. Here we develop semianalytic results that explain the new features observed. Section IV discusses a qualitative description of the dynamics in terms of vortex motion. Section V analyzes other, more general, bias current distributions, showing that our conclusions are characteristic of any bias distribution that concentrates current at the junction edges. Section VI summarizes the main results of the paper.

II. LONG JOSEPHSON JUNCTIONS AND NONUNIFORM CURRENT BIAS

Figure 1 shows a typical planar geometry Josephson junction. The barrier (indicated in gray) is in the same plane as the thin-film electrodes. This geometry is very uncommon in low-T_C junctions where the electrodes and barrier are most often deposited sequentially as a trilayer, resulting in a stacked configuration. However it is a natural configuration for many types of high-T_C junctions, where, for instance, the barrier may be formed by a crystalline grain boundary in an otherwise continuous thin film.[1] The length scale that determines whether the dimensions in directions perpendicular to the transport current should be considered large or small is the Josephson penetration depth λ_J. When one of these dimensions is larger than λ_J, the superconducting phase difference across the junction depends on position in that direction due to magnetic fields generated by the transport currents. The dimension L in the figure indicates the direction in which this planar junction is large (or long). The differential equation that describes the position- and time-dependent phase can be derived[6] by combining Maxwell's equations and the Josephson relations. In many cases, and in particular in HTSC junctions, only one of these dimensions is large with respect to λ_J. Even in this situation, the coupled electrodynamic and superconducting properties can be summarized in a simple differential equation for only a few geometries: in other instances a full three-dimensional analysis of the electric and magnetic fields must be made. Although the planar geometry of Fig. 1 is not one for which a differential equation can be written exactly, it differs in only minor ways from the overlap geometry for which the differential equation[6]

$$\varphi_{xx} - \sin\varphi = \varphi_t - j(x) \tag{1}$$

describes the space and time dependence of the phase difference φ. Here x is the position along the junction length nor-

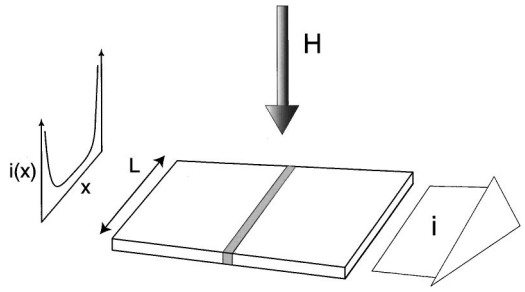

FIG. 1. Schematic view of a typical planar Josephson-junction geometry. The region is shaded gray. Transport current (I) is in the plane of the film, and magnetic field (H) is applied perpendicular to the film plane. The parameter L indicates the long dimension of the barrier. The planar geometry results in a nonuniform bias current distribution in the electrodes (indicated at left), leading to resonancelike features in the IV characteristic.

malized to λ_J, t is the time in units of $\hbar/2eJ_cAR_n$, and $j(x)$ represents the bias current density distribution in the electrode normalized to the junction critical current density. The boundary conditions at the junction edges are $\varphi_x = h \equiv 4\pi H_{\rm app}\lambda_L\lambda_J/\Phi_a$. Equation (1) is valid for the overdamped limit of negligible junction capacitance applicable to most HTSC junctions.

Because the superconducting electrodes are generally thin films of thickness comparable to the London penetration depth λ_L and widths much wider than λ_L, the current flow in them is nonuniform (as indicated schematically in Fig. 1). A configuration with current concentrated near the edges of the film and depleted near the center is known[7] to minimize the energy, although the exact form has not been expressed analytically.[8] It has long been known that such nonuniform electrode bias current can reduce the zero-field junction critical current.[10] It has also recently been shown[9] that the magnetic-field dependence of the measured critical current as well as the shape of the IV characteristic are modified by a nonuniform bias.

First we consider the limiting case where the bias current is concentrated entirely at the junction ends: $j(x) = \delta(x + l/2)il/2 + \delta(x - l/2)il/2$, where $i = I/J_cA$ and $l = L/\lambda_J$ is the normalized junction length. We find that this current distribution reproduces the features found in the more complicated bias distributions of Sec. IV, and can be easily analyzed. Since both $\sin\varphi(x)$ and $\varphi_t(x)$ are continuous functions, integrating Eq. (1) from $-l/2$ to $-l/2+\varepsilon$ gives $\varphi_x(-l/2+\varepsilon) - \varphi_x(-l/2) = -il/2$, or $\varphi_x(-l/2+\varepsilon) = h - il/2$ after substituting the boundary condition. A similar analysis at the other end of the junction gives $\varphi_x(l/2-\varepsilon) = h + il/2$. The interior region can then be described by

$$\varphi_{xx} - \sin\varphi = \varphi_t; \begin{cases} \varphi_x(-l/2) = h - il/2 \\ \varphi_x(+l/2) = h + il/2, \end{cases} \qquad (2)$$

since the bias current is zero in the interior. Equation (2) is identical to that derived for the overdamped in-line geometry,[6] although here it describes an overlap geometry junction with nonuniform bias current. It can clearly be extended to the case where a fraction of the bias current is concentrated at the edges, and the rest uniformly distributed along the junction. This is numerically equivalent to phenomenologically mixing in-line and overlap boundary conditions.[10]

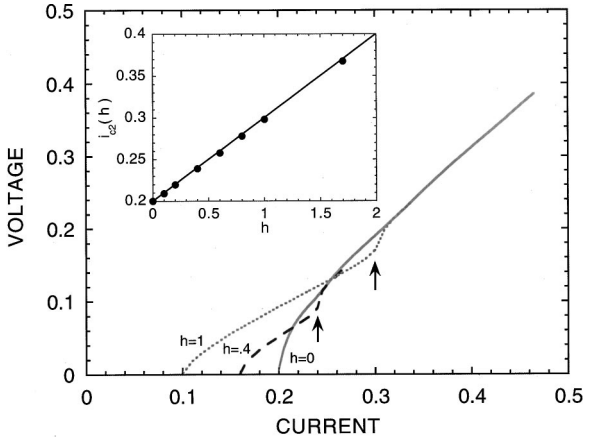

FIG. 2. Numerically-simulated current-voltage (IV) characteristic for edge-based planar Josephson junction for applied magnetic fields of $h = 0$, 0.4, and 1. Note the field-dependent structure in the IV indicated by the arrows. The inset shows bias current at which this structure occurs to depend linearly on applied field.

The *underdamped* equivalent of Eq. (2) has been discussed extensively in the context of inline junction.[11] However, the *overdamped* limit represented by Eq. (2) has received little attention. This is in part due to the limited prospect for applications before the advent of HTSC materials. In Sec. III we discuss IV characteristics derived from Eq. (2). We find that the characteristics are qualitatively different from the underdamped limit. In Sec. IV, we show that more physically realistic current distribution also display these features, and argue that origin of the features is explained by the simplified distribution discussed in Sec. III.

III. *IV* STRUCTURE IN EDGE-BIASED JUNCTIONS

A. Voltage and supercurrent features

Figure 2 shows the numerically simulated IV characteristics resulting from Eq. (2) for applied magnetic fields of $h = 0$, 0.4, and 1.0. The normalized junction length is $l = 20$, and the voltage is averaged over 5000 normalized time units after waiting an ''equilibration'' time of 1000 time units. Two distinct features are observed. The first is a decrease in the critical current in applied magnetic field. This effect is well known and can be shown[6] analytically to obey $i_c(h) = 2l^{-1}(2-h) = i_c(0) - 2h/l$ for $l \gg 1$ (here $i_C(0) = 0.2$ for $l = 20$). However, there is additional structure in the IV in the dissipative state at *another* characteristic current i_{c2}. The inset to Fig. 2 shows that $i_{c2}(h) \sim i_c(0) + 2h/l$. We have verified that this behavior occurs even for $h \sim 5$. This structure has been previously reported[7] for a different nonuniform bias distribution, but its origin was not identified.

This feature is made clearer in Fig. 3, which shows the total time-average supercurrent as a function of bias current for $h = 0$ and $h = 1$ along with the short-junction resistively shunted-junction (RSJ) behavior[6] (dashed line). The $h = 0$ curve generally follows RSJ behavior, apart from excess current and subtle oscillatory structure. Here the supercurrent carried by the junction increases with bias current below i_C.

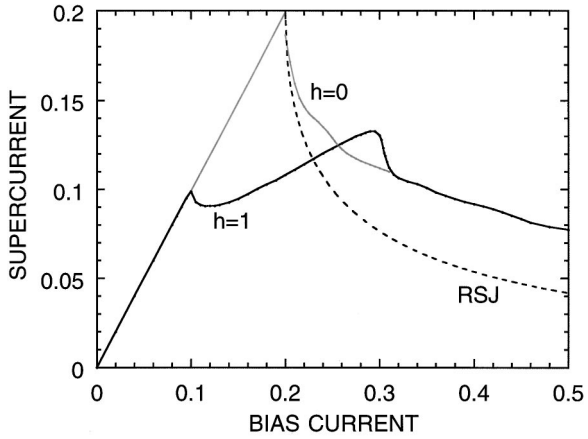

FIG. 3. Total time-averaged supercurrent as a function of bias current for $h=0$ and $h=1$. The dashed line shows the short-junction RSJ behavior. The supercurrent becomes approximately field independent for $i>i_{c2}(h)$, but still differs from the short-junction (RSJ) behavior.

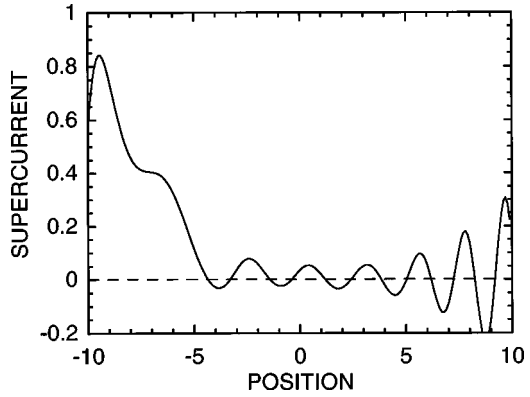

FIG. 4. The local time-averaged supercurrent as a function of position x along the junction for $h=1$ and $i=0.28\,(i_C<i<i_{C2})$. Supercurrent is concentrated at the left edge of the junction.

After the critical current is exceeded and the junction is in the dissipitative state, the supercurrent decreases with increasing bias current as the normal current increases. However, for $h=1$ the supercurrent carried by the junction increases even *above* the critical current $i_C(h=1)=0.1$ in a way similar to $i<i_C$. Only for $i>i_{C2}$ does the supercurrent continually decrease. The sharp drop in supercurrent at i_{C2} is similar to that at i_C, suggesting a similar instability. Although the structure in these curves resembles resonance effects in underdamped junctions,[12] we show here that they are due to dynamical instabilities.

B. Analysis

The behavior described in the previous section results from instabilities at the two junction edges: $i_c(h)$ arises from an instability at $x=+l/2$, and $i_{c2}(h)$ from one at $x=-l/2$. It is well known that the critical current $i_c(h)$ is associated with a transition from a static, nondissipative state to a time-dependent, dissipative state. We have found that $i_{c2}(h)$ represents a transition between *two different* well-defined dissipative states. This transition can be attributed to a dynamical instability in the supercurrent distribution concentrated at the junction end $x=-l/2$. Despite the time-average voltage drop along the entire junction for $i_c(h)<i<i_{c2}(h)$, this region of the junction behaves approximately as the end of a long junction in the *superconducting* state in this current range, while the rest of the junction shows usual dissipative behavior.

A qualitative description is straightforward. For zero-bias current, the applied field induces a circulating ''Meissner'' shielding current, positive at $x=+l/2$ and negative at $x=-l/2$. The behavior for increasing bias current is well known:[6] the bias current adds to the (positive) Meissner supercurrent at $x=+l/2$, while it cancels the (negative) Meissner current at $x=-l/2$. At $i_c(h)$, the supercurrent carried near $x=-l/2$ has increased from its (negative) $i=0$ value to a value near zero, and the supercurrent near $x=+l/2$ has reached its maximum value. Beyond this point the phase distribution becomes time-dependent and a nonzero voltage appears across the junction. If one were to ignore the voltage drop and time-dependent properties of the junction for $i_c(h)<i<i_{c2}(h)$, the same line of reasoning would predict that the supercurrent carried near $x=-l/2$ would continue to increase with bias current until it reached a critical configuration identical to that at $i_c(h)$ near $x=+l/2$. This would be the second instability, and would occur at $i_c(0)+[i_c(0)-i_c(h)]=i_c(0)+2h/l$ because the field-induced Meissner currents are of opposite sign but equal magnitude at the two ends. This is consistent with the data of Figs. 2 and 3.

However, the junction is *not* superconducting in this current range. In particular, the phase distribution is time dependent, and a voltage appears across the junction at all positions. Even so, we find that the supercurrent and phase distribution at $x=-l/2$ closely resembles the end of a *superconducting* junction at each instant in time. In the rest of this section, we present a detailed analysis of the transition in junction properties at $i_{c2}(h)$ in order to understand this mixture of dynamic and pseudostatic configurations in the junction.

To investigate these effects, we spatially resolve the junction dynamics. The time-average voltage does not indicate spatially resolved junction dynamics as it is spatially uniform. However, the time-average supercurrent $i_s^{\rm ave}(x)$ has no such limitations. This allows us to identify the regions of the junction that dominantly contribute to the supercurrent and hence control the IV characteristic. As junction properties for $i<i_c$ have been extensively analyzed,[13] we concentrate on the region $i_c<i<i_{c2}$ and the i_{c2} transition.

Figure 4 shows the *time average* $i_s(x)$ for $i_c<i<i_{c2}$. Although oscillatory structure is observed throughout the junction length, the supercurrent is clearly concentrated near $x=-l/2$. The nonzero voltage across the junction indicates that the phase difference $\varphi(x)$ increases in time through $\varphi_t=v(t)$, and in particular passes continuously through many multiples of 2π at all points along the junction. This corresponds to a supercurrent oscillating between positive and negative values $[i_s\propto\sin(\varphi(x,t))]$. Small values of $i_s^{\rm ave}(x)$ indicate nearly sinusoidal supercurrent oscillations, and corresponding time linear $\varphi(t)$. $i_s^{\rm ave}(x)\approx 1$ implies that $\varphi(t)$ must be very nonsinusoidal, almost steplike, with φ jumping quickly between approximately time-independent values.

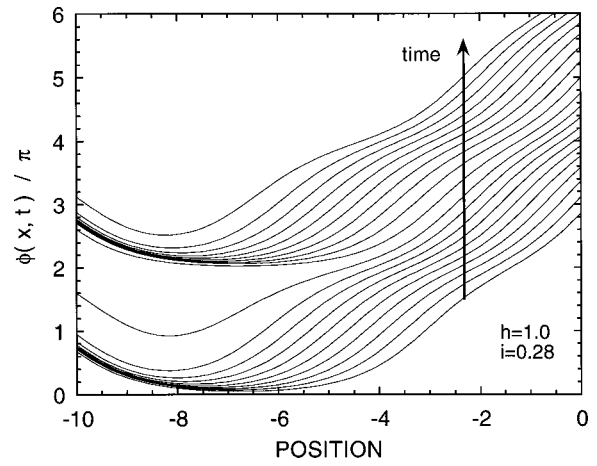

FIG. 5. The phase difference $\varphi(x,t)$ at equally spaced time intervals ($h=1$ and $i=0.28[i_C<i<i_{C2}]$). $\varphi(x,t)$ is approximately static for extended time intervals at the left edge of the junction, and leads to excess supercurrent carried here.

This is explicitly demonstrated in Fig. 5, which shows the phase difference $\varphi(x)$ at equally spaced time intervals. The x range extends from the left end of the junction to the center ($-l/2$ to $x=0$). The phase (and hence supercurrent) distribution is approximately *static* ($\varphi_t \approx 0$) for extended periods of time near the junction edge, while it has an approximately uniform time dependence for x more than $\sim 4\lambda_J$ from the junction edge. Our numerical calculations indicate that this behavior is preserved for all $i<i_{c2}$. Above i_{c2} the supercurrent distribution is characteristically different, as shown in Fig. 6. We discuss this regime further after establishing the nature of the threshold current i_{c2}.

The weak time dependence of $i_s(x)$ near $x=-l/2$ permits a static analysis to be approximately applied. The phase distribution shown near the junction edge in Fig. 5 for $i=0.28 > i_c$ is in fact very like the static solution for a semi-infinite junction for that current: decaying approximately exponentially away from the edge while meeting the boundary conditions. In this region $\varphi(x)$ satisfies Eq. (2) with $\varphi_t \approx 0$.

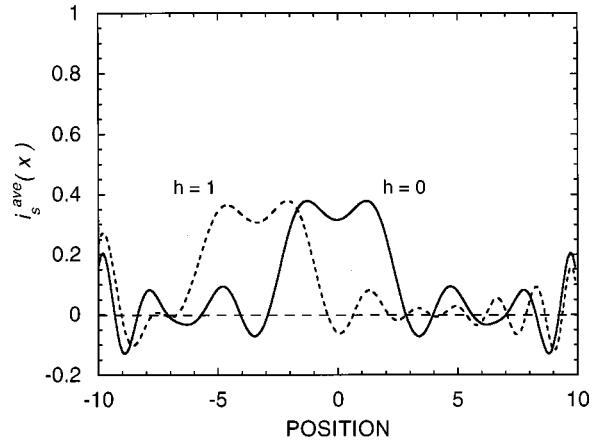

FIG. 6. Local time-averaged supercurrent as a function of position x along the junction for $i=0.4$ and magnetic fields of $h=0$ and $h=1$ [$i>i_{c2}(h)$]. The shape of the dominant supercurrent contribution in the junction interior is independent of field, and leads to the field independence of the *IV* characteristic for $i>i_{c2}(h)$.

Equation (5) can be integrated with respect to φ to obtain $\varphi_x = -\sqrt{2(K-\cos\varphi)}$. The integration constant is found to be $K=1$ by the condition $\varphi_x \to 0$ for $\varphi \to 0$ in the interior of the junction. The maximum current, found by minimizing φ_x at the junction edge, is easily seen to occur for $\varphi(-l/2)=\pi$. Then $i_{c2}(h)=2l^{-1}(2+h)=i_c(h=0)+2h/l$ is obtained by substituting the boundary condition $\varphi_x(-l/2)=h-il/2$, as observed in Fig. 2. The above equation for φ_x also predicts a value for the phase at the end of the junction using the boundary condition $\varphi_x(-l/2)=h-il/2$. This corresponds to $\varphi(-l/2)=2.24=0.71\pi$ for $i=0.28$ and $h=1$. This compares favorably to that shown in Fig. 5, demonstrating that the static phase configuration near the junction end is in fact very similar to that found in a *superconducting* semi-infinite junction. The junction approximately incorporates the static solution at $x=-l/2$, while giving an approximately linear time dependence ($v(x,t)\approx v_s^{\rm ave}(x), i_s^{\rm ave}(x)\approx 0$) to the phase distribution over the rest of the junction. The interpolation between these two solutions occurs in a complicated way that we have not attempted to describe, but which does not seem to strongly influence our conclusions.

$i_{c2}(h)$ can then be associated with a loss of the approximately static phase distribution at $x=-l/2$. Figure 3 shows that this is also associated with an abrupt decrease in the supercurrent carried by the junction, and corresponding voltage (or normal current) increase. Above i_{c2}, the total time-average supercurrent has approximately the same bias current dependence as for $h=0$. The reason for this can be seen in Fig. 6, which shows $i_s^{\rm ave}(x)$ for bias current $i=0.4$ and both $h=0$ and $h=1$. Both show that the local contributions to the total supercurrent are dominated by a narrow region of the junction. This region is exactly at the junction center for $h=0$, and slightly off-center for $h=1$ at this bias current. It moves from the center to the edge as i is decreased, but its shape and hence contribution to the supercurrent is remarkably independent of applied field.

IV. VORTEX DYNAMICS

In many situations the dynamics of long Josephson junctions can be qualitatively understood in terms of the nucleation and motion of Josephson vortices. This is a particularly useful approach in underdamped junctions, where the phase and current distributions that define vortices are of limited spatial extent and hence well separated. As can be seen in Fig. 5, the 2π phase change representing a Josephson vortex at the fields and currents discussed here does *not* occur abruptly as in underdamped junctions, but rather gradually in an almost linear dependence of phase on position.

Nevertheless, an interpretation based on the motion of isolated vortices can qualitatively represent the data. This vortex interpretation is difficult to quantitatively substantiate for the reasons discussed above, and should be used with caution. The instabilities discussed in Sec. III can be viewed as vortex nucleation at the junction edges, and subsequent vortex motion toward the junction center. In zero magnetic field, the critical current represents nucleation or depinning of a vortex at $x=+l/2$ and an antivortex (opposite circulation) at $x=-l/2$. The transport current causes these to flow oppositely toward the junction center where they annihilate. This symmetry enforces the zero-field condition of no net

magnetic flux in the junction. Figure 6 shows the time-average supercurrent for this process: the ''bump'' occurs at the annihilation point.

For nonzero applied field, the situation is more complicated. The two instabilities $i_c(h)$ and $i_{c2}(h)$, respectively, represent vortex and antivortex nucleation-depinning. For $i_c < i < i_{c2}$, a vortex nucleates at $x=+l/2$ and flows across the junction to annihilate at $x=-l/2$ with a nucleating antivortex. Figure 5 indicates that the phase at $x=-l/2$ has a very nonuniform time dependence, characteristic of the annihilation process. For $i>i_{c2}(h)$, our analysis of the time and space dependence of the junction phase suggests that a vortex first nucleates at $x=+l/2$, followed later by antivortex nucleation at $x=-l/2$. Both subsequently flow toward the junction center at the same velocity. Their annihilation point is off-center due to their different starting times. Figure 6 shows the resulting time-average supercurrent distribution. The supercurrent bump is again at the (off-center) annihilation point.

The field independence of this feature (discussed at the end of Sec. III B), and the subsequent field independence of the IV characteristic for $i>i_{c2}(h)$, can be qualitatively understood within the vortex interpretation: as long as annihilation occurs in the junction interior, the annihilation process should be similar and hence produce a similar contribution to the net time-average supercurrent.

V. GENERALIZATIONS

A. Other bias-current distributions

As discussed in Sec. II, the planar geometry typical of high-T_C junctions results in a bias-current distribution that is not precisely equivalent to the edge-biased (symmetric, in-line) configuration that was used in Secs. III and IV. A more physical distribution will have current distributed throughout the junction, with some fraction peaked at the edges. In this section we investigate three bias distributions which more closely approximate the actual current distribution in a planar junction. All show a resonancelike feature, indicating that it is a general property of nonuniform bias, and not unique to a particular distribution.

The first distribution investigated here is a superposition of the in-line (edge-biased) and overlap (uniform) distributions. It been successfully used in studies of the static[10] and dynamic properties[14] of underdamped, long trilayer junctions. Although it interpolates between the edge-bias and uniform distributions, it always has a discontinuity at the edge.

Various analytical expressions have been used which concentrate current at the edges while retaining a smooth current distribution.[6] We investigate two of these. The first[6] uses a parameter γ to characterize the crossover from edge-bias to uniform bias as $I/I_0=(\gamma/l\sinh\gamma)\cosh(2\gamma x/l)$; larger γ gives larger edge current, with $\gamma=0$ corresponding to a uniform current distribution. The second[14] (''square root'') distribution, $I=(I_0/\pi)(l^2/4-x^2)^{-1/2}$, is derived from the macroscopic electrostatics of the superconducting thin film, and has no adjustable parameters.

To describe the linear superposition of in-line (edge-biased) and overlap (uniform) distributions, we define a factor A as the ratio of the fraction of current in the δ functions at the ends to the remainder of the current which is distributed uniformly over the length of the junction. $A=1$ corresponds to the complete edge bias, while $A=0$ describes the uniform bias. Figure 7 shows the time-average supercurrent for various A (offset for clarity) in an applied field $h=1$ (1/2 of h_{co}). The dotted lines indicate the corresponding $h=0$ supercurrent. It should be compared to Fig. 3, which presents the $A=1$ (edge-bias) case in detail. A second critical current (i_{c2}) is observed in the calculated IV curves for all $A\neq 0$, and its dependence on field h remains roughly linear. Although the features become broad for small A (more uniform bias distribution), they remain easily recognizable.

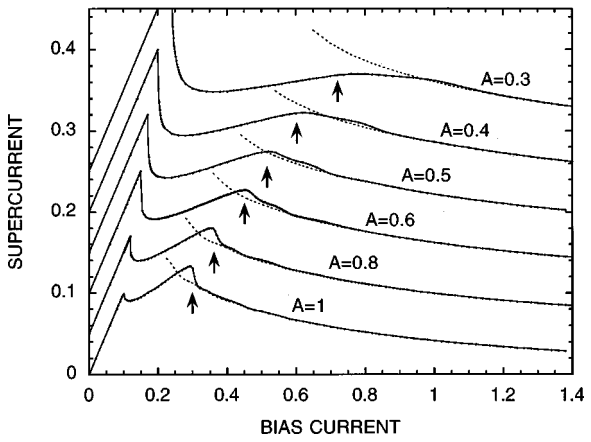

FIG. 7. The supercurrent as a function of bias current for the ''mixed'' distribution in an applied field $h=1$, junction length $l=20$. Each curve is offset by 0.05 units of supercurrent. The vertical arrows indicate $i_{c2}(h=1)$ predicted by the analysis in the text. $A=1$ corresponds to complete edge bias; $A=0$ is the uniform current distribution. Dashed lines are for $h=0$.

The vertical arrows in Fig. 7 indicate $i_{c2}(h=1)$ determined from an analysis similar to that of Sec. III B. When Eq. (5) is integrated with respect to φ for the ''mixed'' bias distribution, and evaluated at the junction end using the boundary conditions in Eq. (2), one finds

$$(i^e l/2 \pm h)^2/2=[1-(i^m)^2]^{1/2}+i^m \arcsin i^m - i^m\varphi_e-\cos\varphi_e$$

for a semi-infinite junction where $\sin\varphi=i^m$ for large x. Here $i^e=iA$ is the edge current, $i^m=i(1-A)$ is the component of uniform bias, and φ_e is the phase at the junction edge. We find $\varphi_e(i_c)=\pi-\arcsin i_c^m$, so that critical values of current are implicitly determined by

$$(i_c^e l/2 \pm h)^2/2=[1-(i_c^m)^2]^{1/2}+i_c^m \arcsin i_c^m - i_c^m\pi. \quad (3)$$

Equation (3) evaluated using the $+$ gives $i_c(h)$ for varying A that corresponds to within a few percent of those determined from the data of Fig. 7. Using $-$ in Eq. (3) predicts an i_{c2} indicated by the vertical arrows of Fig. 7. For $A\geqslant 0.4$ these closely correspond to the point at which the supercurrent decreases for the second time (and hence the threshold for a second increase in normal current). In correspondence with the perspective of Sec. III, this is due to an instability in the phase distribution at the junction end. The agreement is not as good for $A<0.4$: as the bias current distribution becomes more uniform, we may expect that the junction edges act less independently from the junction interior, leading to differences with the simple theory.

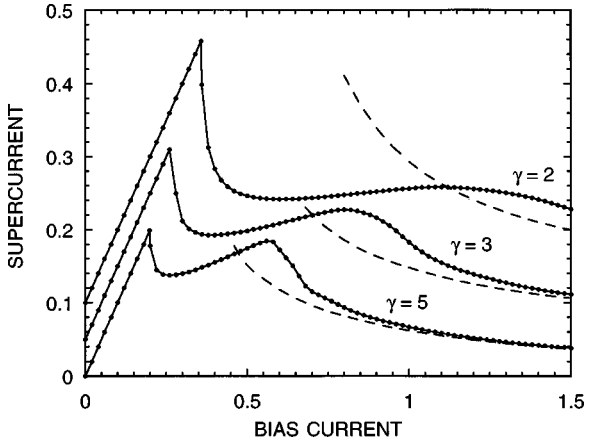

FIG. 8. Supercurrent as a function of bias current for the cosh distribution in an applied field $h=1$, junction length $l=20$. Each curve is offset by 0.05 units of supercurrent. Large γ concentrates current at the edges. $\gamma=0$ corresponds to a uniform current distribution. Dashed lines are for $h=0$.

Figure 8 shows the simulated supercurrent as a function of bias current for the ''cosh'' distribution $I/I_0 = (\gamma/l \sinh\gamma)\cosh(2\gamma x/l)$ discussed above at an applied field $h=1$ and for various values of the edge concentration parameter γ (offset for clarity). Clear supercurrent features are observed for all γ values, although the supercurrent no longer has an abrupt decrease. The features become less distinct as the distribution becomes more uniform.

Figure 9 shows the simulated supercurrent as a function of bias current for the square-root distribution $I = (I_0/\pi)(l^2/4-x^2)^{-1/2}$ for applied magnetic fields $h=1$, 3, and 6. Again a clear supercurrent peak is observed: with increasing field the peak becomes broader, and the corresponding bias current for peak supercurrent increases.

For these more general bias current distributions, we somewhat arbitrarily define $i_{c2}(h)$ as the bias current at which the supercurrent peak is observed. This is consistent with our Sec. III analysis of the edge-bias case due to the abrupt drop in supercurrent at $i_{c2}(h)$, and can be clearly identified for the more general bias distributions. Figure 10 shows the dependence of this $i_{c2}(h)$ on applied magnetic field for all bias distributions (offset for clarity) investigated here. All are roughly linear in field, with slopes approximating that found in Sec. III for the edge-bias case.

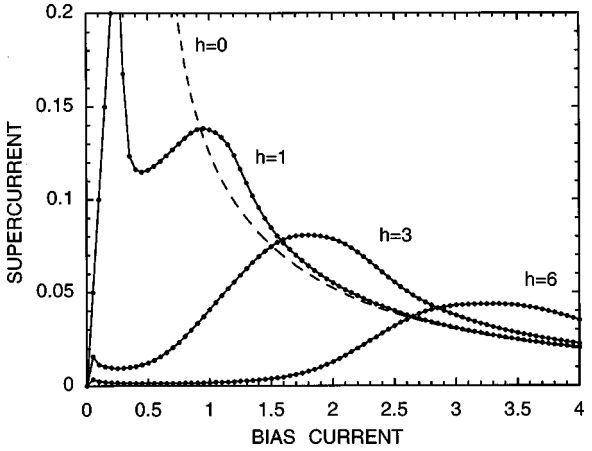

FIG. 9. Supercurrent as a function of bias current in various applied fields h for the square-root distribution, junction length $l=20$.

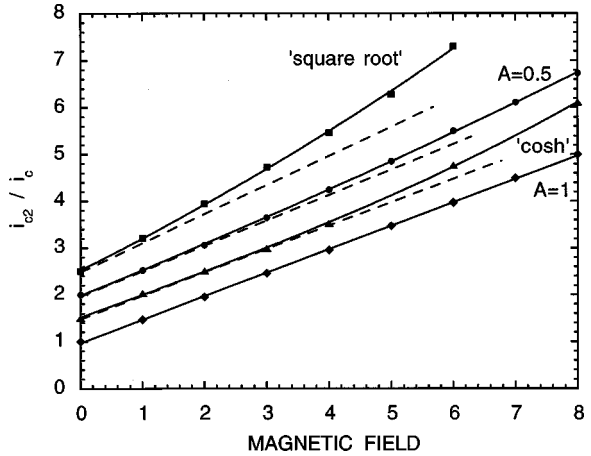

FIG. 10. $i_{c2}(h)$ for all bias distributions. Curves are offset by 0.05 units for clarity. The dashed line for each distribution is the Sec. III result $i_{c2}(h)/i_c(0)=1+h/2$.

The results of this section show that the supercurrent features reported here exist for several different bias distributions that concentrate current at the junction edges. Further, the dependence of i_{c2} on applied field approximately follows the edge-bias analysis of Sec. III, $i_{c2}(h)/i_c(0)=1+h/2$ for $l=20$.

B. Excess current

Many experimental long junction measurements show an ''excess current,'' i.e., extrapolation of the linear (high bias) section of the IV curve to positive values of current. This is observed in zero as well as nonzero applied field. Excess current can readily be incorporated into the resistively-shunted junction (RSJ) form of the IV curves for overdamped Josephson junctions[6] by shifting the IV curve along the current axis. The RSJ expression then becomes $\overline{v} = \sqrt{(i-i_{xs})^2-1}$, where $\overline{v}$ is the time-averaged voltage normalized to the junction I_cR_n, i is the bias current normalized to the junction critical current, and i_{xs} is the normalized ''excess current.'' This model fits our calculated zero-field edge-bias $(A=1)$ IV curves quite well. Below $l\approx10$ no excess current is present. Excess current develops for $l>10$, saturating at a value around 55% for $l>25$. Here we have fit the IV curves out to a voltage five times the apparent I_cR_n, a common experimental criterion.

VI. CONCLUSIONS

We have shown that resonancelike features arising in the IV characteristics of nonuniformly biased overdamped planar Josephson junctions in a magnetic field are in fact due to dynamical instabilities in the phase distribution. The IV features are caused by a transition between two well-defined dissipative states, and occur at a critical bias current i_{c2} that increases linearly with magnetic field. These states can be characterized by the behavior of the junction at its ends: for a region of bias current $i_c<i<i_{c2}$ the junction is in the dissipative state, but one of the ends very accurately retains the

phase and supercurrent distribution of the superconducting state. This configuration is unstable for $i > i_{c2}$, and the dissipation abruptly increases, with a corresponding decrease in supercurrent, to values found for the zero-field characteristic. A qualitative interpretation in terms of vortex motion shows consistency with this model.

These results are of particular importance to high-T_C junctions, which are often fabricated in a planar geometry and hence susceptible to nonuniform bias current distributions. The extreme case of complete edge-bias results in well-defined magnetic-field-dependent features. As the bias current distribution is modified to incorporate a more gradual decrease from the junction ends, the *IV* features also become broader and less well-defined. However, they remain clearly identifiable, centered at values of bias current that depend linearly on applied magnetic field. We attribute this to a common origin of these features, indicating that our analysis carries over to more general bias current distributions.

ACKNOWLEDGMENT

The work was supported by the NSF MRSEC program Award No. DMR-96-32537.

*Electronic address: mark@cheddar.physics.wisc.edu

[1] R. Gross, in *Interfaces in Superconducting Systems*, edited by S. L. Shinde and D. Rudman (Springer, New York, 1992), p. 176.

[2] B. M. Hinaus, M. S. Rzchowski, B. A. Davidson, J. E. Nordman, K. Siangchaew, and M. Libera, Phys. Rev. B **56**, 10 828 (1997); B. A. Davidson, J. E. Nordman, B. M. Hinaus, M. S. Rzchowski, K. Siangchaew, and M. Libera, Appl. Phys. Lett. **68**, 3811 (1996); S. K. Tolpygo *et al.*, *ibid.* **63**, 1696 (1993); W. E. Booij, A. J. Pauza, E. J. Tarte, D. F. Moore, and M. G. Blamire, Phys. Rev. B **55**, 14 600 (1997).

[3] B. D. Hunt, M. G. Forrester, J. Talvacchio, J. D. McCambridge, and R. M. Young, Appl. Phys. Lett. **68**, 3805 (1996); M. A. J. Verhoeven, G. J. Gerritsma, H. Rogalla, and A. A. Golubov, *ibid.* **69**, 848 (1996).

[4] E. Zeldov, John R. Clem, M. McElfresh, and M. Darwin, Phys. Rev. B **49**, 9802 (1994); Ernst Helmut Brandt and Mikhail Indenbom, *ibid.* **48**, 12 893 (1993).

[5] E. Zeldov, A. I. Larkin, V. B. Geshkenbein, M. Konczykowski, D. Majer, B. Khaykovich, V. M. Vinokur, and H. Shtrikman, Phys. Rev. Lett. **73**, 1428 (1994); Maamar Benkraouda and John R. Clem, Phys. Rev. B **58**, 15 103 (1998).

[6] A. Barone and B. G. Paterno, *Physics and Applications of the Josephson Effect* (Wiley, New York, 1982).

[7] T. Van Duzer, *Principles of Superconductive Devices and Circuits* (Elsevier, New York, 1981), and references therein.

[8] See, for example, A. T. Dorsey, Phys. Rev. B **51**, 15 329 (1996), and references therein.

[9] M. S. Rzchowski and B. M. Hinaus, Appl. Phys. Lett. **71**, 3010 (1997).

[10] O. H. Olsen and M. R. Samuelson, J. Appl. Phys. **54**, 6522 (1983); E. Sarnelli, S. Pagano, B. Ruggiero, and M. Russo, IEEE Trans. Magn. **27**, 2716 (1991).

[11] For a summary see Ref. 4, Chap. 10.

[12] R. E. Eck, D. J. Scalapino, and B. N. Taylor, Phys. Rev. Lett. **13**, 15 (1964); A. V. Ustinov *et al.*, IEEE Trans. Appl. Supercond. **3**, 2287 (1993); Y. M. Zhang *et al.*, Phys. Rev. B **51**, 8684 (1995).

[13] C. S. Owen and D. J. Scalapino, Phys. Rev. **164**, 538 (1967).

[14] M. R. Samuelson and S. A. Vasenko, J. Appl. Phys. **57**, 110 (1984).